Nano Research
https://doi.org/10.1007/s12274-017-1854-2
Research Article
ISSN 1998-0124
CN 11-5974/O4

Plasmon resonant amplification of a hot electron-driven photodiode

Lang Shen[1,§], Nirakar Poudel[2,§], George N. Gibson[3,5], Bingya Hou[2], Jihan Chen[2], Haotian Shi[4], Ernest Guignon[5], William D. Page[5], Arturo Pilar[5], and Stephen B. Cronin[2,6] (✉)

[1] *Mork Family Department of Chemical Engineering and Materials Science, University of Southern California, Los Angeles, CA 90089, USA*
[2] *Ming Hsieh Department of Electrical Engineering, University of Southern California, Los Angeles, CA 90089, USA*
[3] *Department of Physics, University of Connecticut, Storrs, CT 06269, USA*
[4] *Department of Chemistry, University of Southern California, Los Angeles, CA 90089, USA*
[5] *Ciencia Inc., East Hartford, CT 06108, USA*
[6] *Department of Physics and Astronomy, University of Southern California, Los Angeles, CA 90089, USA*
[§] *Lang Shen and Nirakar Poudel contributed equally to this work.*

Received: 29 May 2017
Revised: 9 September 2017
Accepted: 15 September 2017

KEYWORDS

hot electrons,
plasmonic resonance,
plasmon,
grating,
photocurrent,
non-equilibrium

ABSTRACT

We report plasmon resonant excitation of hot electrons in a photodetector based on a metal/oxide/metal (Au/Al_2O_3/graphene) heterostructure. In this device, hot electrons, excited optically in the gold layer, jump over the oxide barrier and are injected into the graphene layer, producing a photocurrent. To amplify this process, the bottom gold electrode is patterned into a plasmon resonant grating structure with a pitch of 500 nm. The photocurrent produced in this device is measured using 633-nm-wavelength light as a function of incident angle. We observe the maximum photocurrent at ±10° from normal incidence under irradiation with light polarized parallel to the incident plane (p-polarization) and perpendicular to the lines on the grating, and a constant (angle-independent) photocurrent under irradiation with light polarized perpendicular to the incident plane (s-polarization) and parallel to the grating. These data show an amplification factor of 4.6× under resonant conditions. At the same angle (±10°), we also observe sharp dips in the photoreflectance corresponding to wavevector matching between the incident light and the plasmon mode in the grating. In addition, finite-difference time-domain simulations predict sharp dips in the photoreflectance at ±10°, and the electric field intensity profiles show clear excitation of a plasmon resonant mode when illuminated with p-polarized light at this angle.

Plasmon resonance has been used in several applications, including biosensing [1], surface-enhanced Raman spectroscopy [2], and photocatalysis [3, 4], primarily through the effect of local field enhancement. However, the idea of hot electrons excited in metals has been used in photocatalysis [5–9] and solid-state devices [10, 11] recently. Brongersma's group reported hot-electron photodetection by a pla-

Address correspondence to scronin@usc.edu

smonic nanostripe antenna [10]. They used a metal/oxide/metal stack, and photocurrent was generated only when the incident photon energy was larger than the oxide barrier energy. In 2015, Halas's group reported similar measurements, in which the polarization dependence of plasmon resonant devices, with ohmic and Schottky contacts with defect-rich TiO_2, was compared [11]. Several recent theoretical studies have concluded that plasmon resonant excitations can decay into hot electrons in metal nanostructures [12–16], presenting the possibility of engineering useful devices and structures using this effect despite the extremely short lifetimes of hot electrons in metals (~ 10 fs) [17, 18].

Plasmonic grating structures provide a useful and unique platform for studying plasmon resonant phenomena. These nanostructures can be excited using plasmon resonance or nonresonantly (i.e., by bulk metal absorption) by simply varying the polarization of the incident light. These nanostructures enable us to distinguish between plasmon resonant excitation (p-polarization) and nonresonant bulk metal absorption (s-polarization) while keeping all the other variables in the experiment, such as the sample morphology and photon energy, constant. In the work presented here, we study amplification of a hot electron-driven photodetector using a plasmon resonant grating. The angle dependence of the photocurrent is correlated with the photoreflectance to verify the conditions for resonant excitation of the plasmon mode. Electromagnetic simulations are used to further verify the nature of this amplification and predict further enhancement in alternative grating configurations.

In this work, metal gratings are fabricated by first etching a silicon wafer using reactive ion etching. This creates a corrugated surface with a pitch of 500 nm. Then, a 50-nm gold film is deposited on top of this structure, with a 3-nm Ti adhesion layer between the silicon and the gold [19]. A scanning electron microscope (SEM) cross-sectional image of one of these gratings is shown in Fig. 1(a). Next, a 5-nm Al_2O_3 film is deposited using atomic layer deposition. Monolayer graphene is grown by chemical vapor deposition on copper foil at 1,000 ˚C in methane gas. After growth, the copper foil is spin-coated with

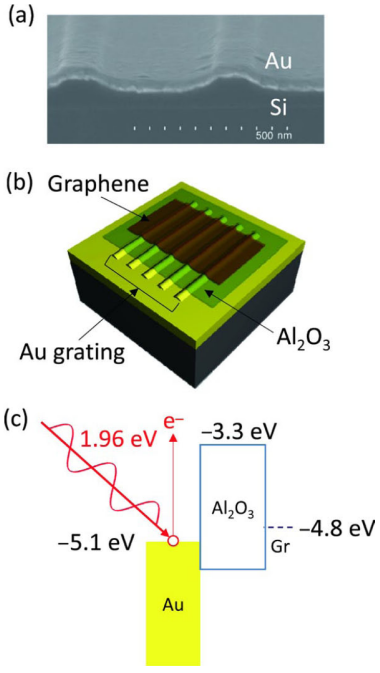

Figure 1 Illustrations of plasmon resonant grating structure. (a) Cross-sectional SEM image and (b) schematic. (c) Energy band diagram with respect to vacuum illustrating the mechanism of hot electron injection.

poly(methyl methacrylate) (PMMA-A6) at 2,000 rpm for 45 s and then baked at 150 ˚C for 5 min. The copper foil is then etched away in copper etchant, and the graphene with PMMA is scooped out and rinsed in 10% HCl and deionized water. Next, the monolayer graphene is transferred to the target substrate by the same scooping method, and baked at 120 ˚C for 5 min to improve adhesion. The PMMA layer is then removed by a 5-min acetone dip [20]. The electrical contacts are made directly on top of the exposed Au layer while the Si and Ti are kept out of the circuit. Finally, the sample is mounted on a rotational stage and illuminated with collimated 633-nm-wavelength light, as illustrated in Fig. 2(c). A chopper wheel is used to modulate the light at 200 Hz, and the AC photocurrent is measured using a lock-in amplifier.

Figure 2(a) shows the AC photocurrent as a function of incident angle for light with an intensity of 106 $mW \cdot cm^{-2}$ polarized both parallel and perpendicular to the lines on the grating. Here, we see two peaks appearing at ±10° from normal incidence when the light is polarized parallel to the plane of incidence (p-polarization) and perpendicular to the grating,

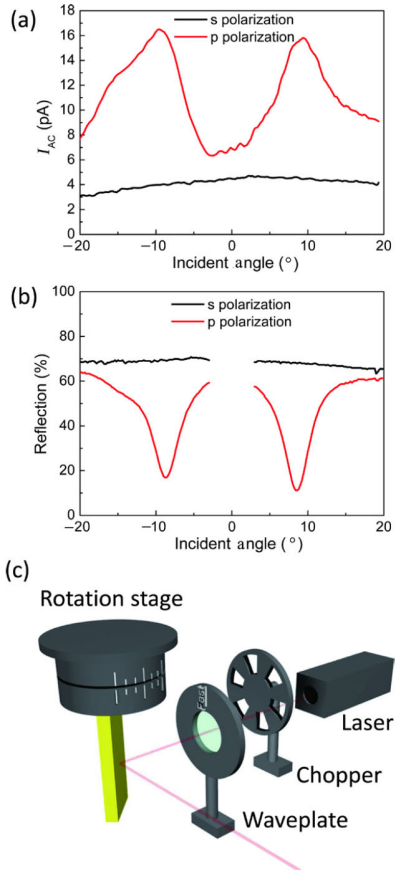

Figure 2 Characterization of the plasmon resonant grating. (a) Photocurrent and (b) photoreflectance as a function incident angle for 633 nm light polarized parallel and perpendicular to the grating structure. (c) Schematic of the experimental measurement configuration.

but a constant (angle-independent) photocurrent when the light is polarized perpendicular to the incidence plane (s-polarization) and parallel to the grating. These data show that the hot electrons are, in fact, amplified by a factor of 4.6× in the metal under resonant conditions. Figure 2(b) shows the photoreflectance as a function of the incident angle, which exhibits sharp dips at ±10° from normal incidence. This is a clear signature of plasmon resonance, which is achieved when there is wavevector matching between the incident light and the plasmon resonant modes in the grating.

To further understand the amplification observed in these plasmon resonant devices, we performed electromagnetic simulations using the finite-difference time-domain (FDTD) method. Figure 3(a) shows the calculated reflectance as a function of incident angle for s- and p-polarized light. As in our experimental measurements, the simulated data exhibit sharp dips at ±10° from normal incidence for p-polarized light and nearly constant reflection for s-polarized light. Figures 3(b) and 3(d) show the electric field intensity distribution along the cross section of these gratings when they are illuminated at normal incidence. Here, we see relatively low electric field intensities corresponding to the absence of coupling to the plasmonic modes. At an incident angle of 10°, however, we clearly see the plasmon resonant mode excited by p-polarized light, which produces an electric field enhancement of approximately 66× at the surface of the metal. Figure 3(c) shows the electric field intensity distribution along the cross section of this grating when it is irradiated at resonance (at 10° with p-polarized light). Here, an intense electric field can be seen, indicating clear excitation of plasmon resonance. Under s-polarized light, however, the field profile looks almost the same as that under normally incident light. The plasmon-enhanced absorption of light in the gold layer leads to generation of more hot electrons and hence a higher photocurrent [10]. Owing to the limited mean free path of hot electrons in the gold layer, only a fraction of the generated electrons can contribute to the photocurrent. Using a literature value of 20 nm for the mean free path of electrons with an energy 2 eV above the Fermi level, we estimate the amplified photoresponse from enhanced light absorption by taking the integral of E^2 within the topmost 20 nm of the gold, as described in Eq. (1) [21]

$$EF = \frac{\int_{f(x,y)-20\text{ nm}}^{f(x,y)} \left|E_{\text{p}}\right|^2 \mathrm{d}x\mathrm{d}y\mathrm{d}z}{\int_{f(x,y)-20\text{ nm}}^{f(x,y)} \left|E_{\text{s}}\right|^2 \mathrm{d}x\mathrm{d}y\mathrm{d}z} \quad (1)$$

where $f(x, y)$ is the profile of the Au top surface. This model predicts a relative p/s-polarization ratio of 5.4× under resonant conditions, which is in good agreement with our experimental findings.

In this work, no attempt was made to optimize the grating structure for maximum amplification; however, simple modifications of the grating, such as changes in the pitch or material, can greatly improve the resonant behavior. As a demonstration, we simulated several alternative grating configurations (i.e., using different pitches and metals). As shown in Fig. 4, using the same configuration and incident light,

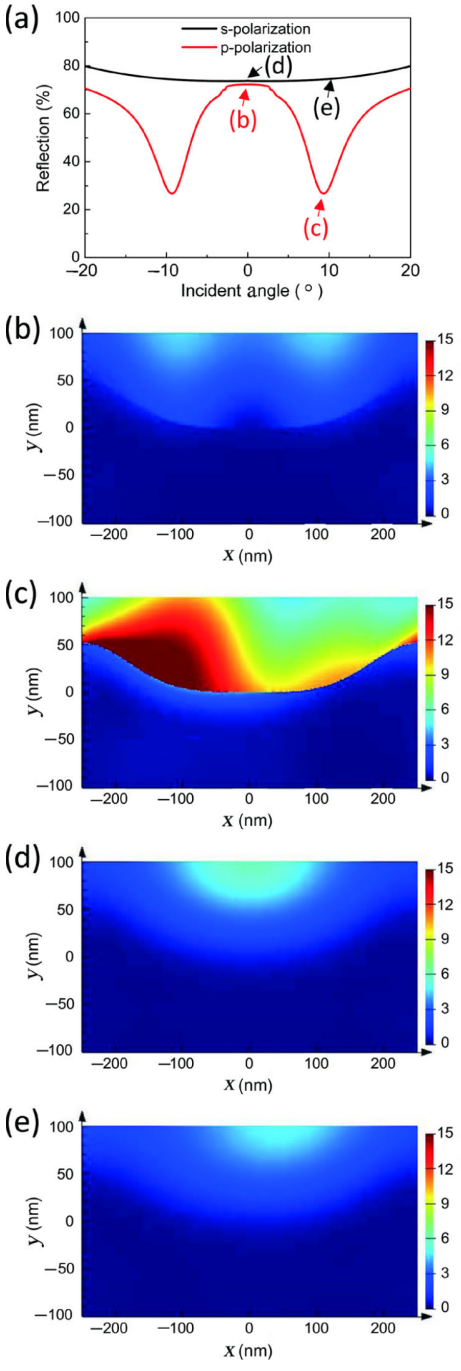

Figure 3 FDTD simulation results for different incident conditions. (a) Simulated photoreflectance as a function of incident angle for p- and s-polarized light. Simulated cross-sectional electric field intensity profiles (E^2) for illumination at ((b), (d)) normal and ((c), (e)) 10° incidence.

the resonant angle can be shifted from 4° to 18° for gold gratings by changing the pitch from 400 to 600 nm. For 400-nm-pitch gratings, the coupling can be made significantly stronger if Au is replaced with Al, as indicated by the much sharper dip and almost

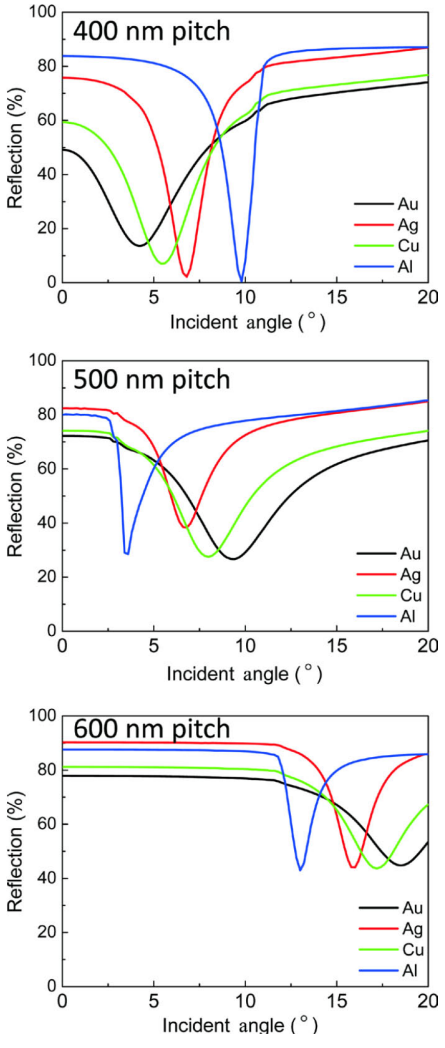

Figure 4 FDTD simulations of reflection of 633 nm light for different metals and pitches at different incident angles.

zero reflection at resonance.

In conclusion, we observe plasmon resonant amplification of hot electrons in a Au/Al_2O_3/graphene photodetector. Here, optically excited hot electrons jump over the oxide barrier, thus producing a photocurrent. In this device configuration, the bottom gold electrode contains a plasmon resonant grating structure in order to increase the photodetection efficiency. Using 633-nm-wavelength light, we observe clear peaks in the photocurrent at an angle of ±10° from normal incidence for light polarized perpendicular to the grating, whereas no modulation of the photocurrent is observed for light polarized parallel to the grating. These data show an amplification factor of 4.6× for hot carrier injection under resonant conditions. Moreover, we observe sharp

dips in the photoreflectance at the same angles, which correspond to good wavevector matching between the plasmon mode in the grating and the incident light. Electromagnetic (FDTD) simulations predict the same reflectance profiles observed experimentally and show clear excitation of a plasmon resonant mode when the structure is irradiated under resonant conditions (i.e., p-polarization at ±10°).

Acknowledgements

This research was supported by NSF Award No. CBET-1512505 (L. S.), Air Force Office of Scientific Research Grant No. FA9550-15-1-0184 (B. H.), Army Research Office (ARO) Award No. W911NF-14-1-0228 (H. S.), Department of Energy (DOE) Award No. DE-FG02-07ER46376 (N. P.), and ACS-PRF grant #55993-ND5 (J. C.).

References

[1] Anker, J. N.; Hall, W. P.; Lyandres, O.; Shah, N. C.; Zhao, J.; Van Duyne, R. P. Biosensing with plasmonic nanosensors. *Nat. Mater.* **2008**, *7*, 442–453.

[2] Fleischmann, M.; Hendra, P. J.; McQuillan, A. J. Raman spectra of pyridine adsorbed at a silver electrode. *Chem. Phys. Lett.* **1974**, *26*, 163–166.

[3] Liu, Z. W.; Hou, W. B.; Pavaskar, P.; Aykol, M.; Cronin, S. B. Plasmon resonant enhancement of photocatalytic water splitting under visible illumination. *Nano Lett.* **2011**, *11*, 1111–1116.

[4] Ingram, D. B.; Linic, S. Water splitting on composite plasmonic-metal/semiconductor photoelectrodes: Evidence for selective plasmon-induced formation of charge carriers near the semiconductor surface. *J. Am. Chem. Soc.* **2011**, *133*, 5202–5205.

[5] Mukherjee, S.; Libisch, F.; Large, N.; Neumann, O.; Brown, L. V.; Cheng, J.; Lassiter, J. B.; Carter, E. A.; Nordlander, P.; Halas, N. J. Hot electrons do the impossible: Plasmon-induced dissociation of H_2 on Au. *Nano Lett.* **2013**, *13*, 240–247.

[6] Mukherjee, S.; Zhou, L. N.; Goodman, A. M.; Large, N.; Ayala-Orozco, C.; Zhang, Y.; Nordlander, P.; Halas, N. J. Hot-electron-induced dissociation of H_2 on gold nanoparticles supported on SiO_2. *J. Am. Chem. Soc.* **2014**, *136*, 64–67.

[7] DuChene, J. S.; Sweeny, B. C.; Johnston-Peck, A. C.; Su, D.; Stach, E. A.; Wei, W. D. Prolonged hot electron dynamics in plasmonic-metal/semiconductor heterostructures with implications for solar photocatalysis. *Angew. Chem., Int. Ed.* **2014**, *53*, 7887–7891.

[8] Robatjazi, H.; Bahauddin, S. M.; Doiron, C.; Thomann, I. Direct plasmon-driven photoelectrocatalysis. *Nano Lett.* **2015**, *15*, 6155–6161.

[9] Hou, B. Y.; Shen, L.; Shi, H. T.; Kepadia, R.; Cronin, S. B. Hot electron-driven photocatalytic water splitting. *Phys. Chem. Chem. Phys.* **2017**, *19*, 2877–2881.

[10] Chalabi, H.; Schoen, D.; Brongersma, M. L. Hot-electron photodetection with a plasmonic nanostripe antenna. *Nano Lett.* **2014**, *14*, 1374–1380.

[11] Zheng, B. Y.; Zhao, H.; Manjavacas, A.; McClain, M.; Nordlander, P.; Halas, N. J. Distinguishing between plasmon-induced and photoexcited carriers in a device geometry. *Nat. Commun.* **2015**, *6*, 7797.

[12] Govorov, A. O.; Zhang, H.; Gun'ko, Y. K. Theory of photoinjection of hot plasmonic carriers from metal nanostructures into semiconductors and surface molecules. *J. Phys. Chem. C* **2013**, *117*, 16616–16631.

[13] Sundararaman, R.; Narang, P.; Jermyn, A. S.; Goddard III, W. A.; Atwater, H. A. Theoretical predictions for hot-carrier generation from surface plasmon decay. *Nat. Commun.* **2014**, *5*, 5788.

[14] Brown, A. M.; Sundararaman, R.; Narang, P.; Goddard III, W. A.; Atwater, H. A. Nonradiative plasmon decay and hot carrier dynamics: Effects of phonons, surfaces, and geometry. *ACS Nano* **2016**, *10*, 957–966.

[15] Narang, P.; Sundararaman, R.; Atwater, H. A. Plasmonic hot carrier dynamics in solid-state and chemical systems for energy conversion. *Nanophotonics* **2016**, *5*, 96–111.

[16] Sakurai, H.; Haruta, M. Synergism in methanol synthesis from carbon dioxide over gold catalysts supported on metal oxides. *Catal. Today* **1996**, *29*, 361–365.

[17] Brongersma, M. L.; Halas, N. J.; Nordlander, P. Plasmon-induced hot carrier science and technology. *Nat. Nanotechnol.* **2015**, *10*, 25–34.

[18] Clavero, C. Plasmon-induced hot-electron generation at nanoparticle/metal-oxide interfaces for photovoltaic and photocatalytic devices. *Nat. Photonics* **2014**, *8*, 95–103.

[19] Rice, J. M.; Stern, L. J.; Guignon, E. F.; Lawrence, D. A.; Lynes, M. A. Antigen-specific T cell phenotyping microarrays using grating coupled surface plasmon resonance imaging and surface plasmon coupled emission. *Biosens. Bioelectron.* **2012**, *31*, 264–269.

[20] Chen, C. C.; Chang, C. C.; Li, Z.; Levi, A. F. J.; Cronin, S. B. Gate tunable graphene-silicon Ohmic/Schottky contacts. *Appl. Phys. Lett.* **2012**, *101*, 223113.

[21] Sze, S. M.; Moll, J. L.; Sugano, T. Range-energy relation of hot electrons in gold. *Solid-State Electron.* **1964**, *7*, 509–523.